

**The VLA-COSMOS Survey:  
III. Further Catalog Analysis and the Radio Source Counts**

M. Bondi<sup>1</sup>, P. Ciliegi<sup>2</sup>, E. Schinnerer<sup>3</sup>, V. Smolčić<sup>3</sup>, K. Jahnke<sup>3</sup>, C. Carilli<sup>4</sup>, G. Zamorani<sup>2</sup>

**ABSTRACT**

The VLA-COSMOS Large Project has imaged the 2 deg<sup>2</sup> COSMOS field with a resolution of 1.5 arcsec and a sensitivity of about 11  $\mu$ Jy ( $1\sigma$ ) yielding to a catalog of  $\sim 3600$  radio sources. In this paper we present a further analysis of the VLA-COSMOS Large Project catalog of radio sources aimed to: 1) quantify and correct for the effect of bandwidth smearing in the catalog, 2) determine the incompleteness produced by the noise bias and the resolution bias in the new catalog and 3) derive the radio source counts at 1.4 GHz.

The effect of bandwidth smearing on the radio sources in the catalog was quantified comparing the peak and total flux densities in the final mosaic and in each of the individual pointings where the source was closest to the center of the field. We find that the peak flux densities in the original VLA-COSMOS Large Project catalog have to be divided by a factor about 0.8 or 0.9, depending on the distance from the mosaic center.

The completeness of the radio catalog has been tested using samples of simulated radio sources with different angular size distributions. These simulated sources have been added to the radio image and recovered using the same techniques used to produce the radio catalog. The fraction of missed sources as a function of the total flux density is a direct measure of the incompleteness.

Finally, we derived the radio source counts down to 60  $\mu$ Jy with unprecedented good statistics. Comparison to the findings of other surveys shows good agreement in the flux density range 0.06-1 mJy confirming the upturn at  $\sim 0.5$  mJy and a possible decline of the source counts below  $\sim 0.1$  mJy.

*Subject headings:* Surveys – Radio continuum: galaxies – Methods: data analysis

---

<sup>1</sup>INAF - Istituto di Radioastronomia, Via Gobetti 101, I-40129 Bologna, Italy

<sup>2</sup>INAF - Osservatorio Astronomico di Bologna, Via Ranzani 1, I-40127, Bologna, Italy

<sup>3</sup>Max-Planck-Institut für Astronomie, Königstuhl 17, D-69117 Heidelberg, Germany

<sup>4</sup>National Radio Astronomy Observatory, P.O. Box O, Socorro, NM 87801-0387, U.S.A.

## 1. Introduction

In recent years, we have experienced a renaissance of deep radio surveys, usually associated with multi-waveband observational programmes mainly designed to probe the formation and evolution of galaxies and Super Massive Black Holes (SMBH). These surveys, mostly carried out at 1.4 GHz, have enabled the study of sub-mJy and  $\mu\text{Jy}$  radio source populations (hereafter  $\mu\text{Jy}$  population) and in particular the determination, with robust statistics, of the radio source counts down to a few tens of  $\mu\text{Jy}$  (e.g. Hopkins et al. 1998; Richards 2000; Bondi et al. 2003; Ciliegi et al. 2003; Hopkins et al. 2003; Seymour, McHardy & Gunn 2004; Huynh et al. 2005; Prandoni et al. 2006; Fomalont et al. 2006; Simpson et al. 2006; Ivison et al. 2007; Bondi et al. 2007).

While it is clear that the  $\mu\text{Jy}$  population is a mixture of different classes of objects (radio loud and radio quiet AGN, starburst galaxies, spirals), the exact contribution of these different classes to the radio source counts is still not very well established and often dependent on the optical limit of the spectroscopic follow-up (Benn et al. 1993; Hammer et al. 1995; Georgakakis et al. 1999; Gruppioni et al. 1999; Prandoni et al. 2001; Afonso et al. 2005; Fomalont et al. 2006; Simpson et al. 2006). The role played by the cosmological evolution of the different classes of objects is even more uncertain. Recently, Smolčić et al. (2006) have developed a new classification method to separate star forming galaxies and AGN based on photometric rest-frame colors for local galaxy samples. The application of this classification method to the VLA-COSMOS sources (Smolčić et al. 2008a) shows that the radio population above  $\sim 50 \mu\text{Jy}$  is a mixture of roughly 30–40% of star forming galaxies and 50–60% of AGN galaxies, with a minor contribution ( $\sim 10\%$ ) of QSOs.

The international COSMOS (Cosmic Evolution) survey (Scoville et al. 2007a) is designed to probe the correlated evolution of galaxies, star formation, AGN up to high redshift. The survey includes state of the art imaging data covering the entire wavelength range from the X-rays to the radio domain (Hasinger et al. 2007; Zamojski et al. 2007; Taniguchi et al. 2007; Scoville et al. 2007b; Capak et al. 2007; Sanders et al. 2007; Bertoldi et al. 2007; Schinnerer et al. 2004, 2007) supported by extensive optical spectroscopic campaigns using mainly the VLT/VIMOS and the Magellan/IMACS instruments (Lilly et al. 2007; Trump et al. 2007).

The radio observations of the COSMOS field were done with the VLA in A and C configuration and are described in Schinnerer et al. (2004, 2007). The whole  $2 \text{ deg}^2$  field was imaged in mosaic mode with a resolution of 1.5 arcsec. The sensitivity is uniform in the inner  $1 \text{ deg}^2$  with an average rms value of  $10.5 \mu\text{Jy}/\text{beam}$  and it increases almost regularly to the outer regions of the  $2 \text{ deg}^2$  field. From the mosaic a catalog of radio sources, the VLA-COSMOS Large Project Catalog, was extracted. The catalog lists  $\sim 3600$  radio sources selected above the local  $4.5\sigma$  threshold over an area of  $2 \text{ deg}^2$ . A full description of

the observations, data reduction and catalog extraction is given in Schinnerer et al. (2007, hereafter S07).

In this paper we present a further analysis on the VLA-COSMOS Large Project Catalog aimed to quantify the impact of bandwidth smearing (Section 2) and the survey completeness (Section 3). Finally, we derive the radio source counts and compare them with those derived from similar surveys (Section 4).

A more detailed interpretation of the radio data is left to other papers which are currently in preparation. In particular, the optical identifications of the VLA-COSMOS radio sources are presented by Ciliegi et al. (2008), the fraction of star-forming galaxies and AGN in the sub-mJy population of the VLA-COSMOS field is discussed in Smolčić et al. (2008a) and the dust un-biased cosmic star formation history is derived from the 1.4 GHz radio data in Smolčić et al. (2008b).

## 2. Bandwidth smearing correction

Bandwidth smearing (or chromatic aberration) affects all synthesis observations made with a finite width of the receiver channels. Imaging sources at large distances from the phase center can yield to radial smearing, increasing the source size and reducing the peak flux density, while the integrated flux density is conserved. The image smearing is proportional to the fractional bandwidth (the bandwidth divided by the central frequency of observation) and to the distance from the phase center in units of the synthesized beam (e.g. Thompson 1999). For single pointing observation the bandwidth smearing simply increases with the radial distance from the phase centre. For a mosaic image, produced by multi-pointing observations, the contribution from all the pointings has to be taken into account and the resulting radial pattern will be much more complicated depending also on the adopted spacing pattern of the individual pointings.

In order to quantify the effect of bandwidth smearing on the VLA-COSMOS observations we ran the same procedure that produced the radio catalog on each of the 23 individual pointings (see S07). For the strongest sources we compared their peak and total flux densities in the final mosaic with the corresponding peak and total flux densities in the pointing where the sources are closest to the field center. The total flux density of each source in the mosaic and in the individual pointings are in very good agreement (the median value of the ratio is 1.03 with an r.m.s. dispersion of 0.04) confirming that the total flux density is properly recovered. On the other hand, as expected for observations affected by bandwidth smearing, the peak flux densities are underestimated in the final mosaic with respect to the

peak fluxes in the individual pointings where the sources are closest to the field center. To quantify this effect we selected only sources which are within a radius  $R_{\min} \leq 5'$  from the field center in, at least, one individual pointing. The peak flux density of a source within  $5'$  from the field center is almost unaffected (less than 5% for the VLA-COSMOS observations) by bandwidth smearing and can be compared with the peak flux in the mosaic. The image of the source in the mosaic is the combination of all the images in the individual pointings where the source is within the cut-off radius ( $16.8'$ , see S07).

In Figure 1 we show the peak flux ratios for compact sources (angular sizes less than  $4''$ ) with peak fluxes brighter than  $0.2$  mJy/beam and  $R_{\min} \leq 5'$  as a function of the radial distance from the center in the final mosaic.

The ratio is about  $0.8 \pm 0.05$  for sources in the inner region of the mosaic, within  $30'$  from the mosaic center. In the region between  $30'$  and  $45'$ , the ratio is  $0.9 \pm 0.03$ , implying a smaller correction in this area. This is due to the fact that the number of overlapping pointings is smaller at larger radii ( see Fig. 2). Within these two regions the effect appears to be independent from the position in the mosaic considering the dispersion of the points. Therefore, we adopted a constant bandwidth smearing correction factor of  $0.8$  for the sources within  $30'$  from the mosaic center and a constant value of  $0.9$  for those between  $30'$  and  $45'$ .

We performed this analysis in the inner  $1 \text{ deg}^2$  ( $1 \times 1 \text{ deg.}$  square region) of the final mosaic since this region has the deepest and most uniform sensitivity and it will be used to derive the source counts in the following Section. Beyond  $45'$  from the mosaic center this correction is no more valid as each source in the mosaic receives a contribution from only one pointing and therefore the bandwidth smearing correction will be a function of the distance from the center of the individual pointing where each source is located, rather than of the distance from the mosaic center.

Consequently, to derive the radio source counts in the inner  $1 \text{ deg}^2$  we divided all the peak flux densities by  $0.8$  or  $0.9$  depending on the distance from the center of the mosaic and derived the new resolved/unresolved criterion following the procedure described in S07. Since the ratio between total and peak fluxes is a direct measure of the extent of a radio source, we used it to discriminate between resolved or extended sources (i.e. larger than the beam) and unresolved sources.

Figure 3 shows the ratio of the total integrated flux density  $S_{\text{total}}$  and the corrected peak flux density  $S_{\text{peak}}$  as function of the signal to noise ratio. To select the resolved sources we have fitted a lower envelope in Fig. 3 which contains  $\simeq 95\%$  of the sources with  $S_{\text{total}} < S_{\text{peak}}$  and mirrored it above the  $S_{\text{total}}/S_{\text{peak}} = 1$  line. The criterion of  $95\%$  of sources contained in the lower envelope of Fig. 3 is slightly different from that used in S07, where a value of  $99\%$

was adopted. We reckon that the value adopted here is the best compromise to properly classify the sources as resolved or unresolved because it fully characterises the shape of the distribution of sources with  $S_{\text{total}} < S_{\text{peak}}$  and, at the same time, it excludes the most extreme values. This envelope is described by the equation

$$S_{\text{total}}/S_{\text{peak}} = 1 + [100/(S_{\text{peak}}/rms)^{2.4}] \quad (1)$$

It is important to note that in Fig. 3 there is no systematic offset from the  $S_{\text{total}}/S_{\text{peak}} = 1$  line at high SNRs. This is an a posteriori confirmation that we adopted an appropriate bandwidth smearing correction. Considering only sources with  $\text{SNR} \geq 5$  in the inner  $1 \text{ deg}^2$ , we obtain 484 resolved sources, for which the total flux is given by the total flux of the Gaussian fitting, and 1208 unresolved ones, for which the total flux is set equal to the peak flux.

It is worth noting a few points regarding the effects of the correction on the VLA-COSMOS Large Project Catalog:

- The correction has been determined only out to a radius of 45 arcmin from the mosaic center and should be safely adopted only in this region.
- The catalog is still selected on the old, pre-bandwidth smearing correction, peak flux densities or signal-to-noise ratio, and we applied the bandwidth smearing correction only to the sources already in the catalog. In the remaining we will refer to the signal-to-noise ratio as the original one, calculated with the uncorrected peak flux density.
- The correction affects the resolved/unresolved classification of a source and therefore also the total flux density and size for the sources, previously classified as resolved, that are found unresolved after correcting for the smearing. This affects about 500 sources, almost one third of the total number of sources in the inner  $1 \text{ deg}^2$  with  $\text{SNR} \geq 5$ .

### 3. Survey completeness

#### 3.1. The visibility area

The VLA-COSMOS Large Project Catalog contains  $\sim 3600$  radio sources extracted from a  $2 \text{ deg}^2$  area. As shown in S07, the noise is not uniform over the whole area and increases in the outer regions. The central  $1 \text{ deg}^2$  area has the lowest and most uniform

noise (mean rms  $10.5 \mu\text{Jy}$ ) and therefore it is very well-suited to derive the source counts. Extending the analysis to the whole area and catalog would increase the number of objects at higher flux densities ( $> 0.1 - 0.2 \text{ mJy}$ ), but it would not add much to the accuracy of the source counts at the lowest flux densities, which is the main focus of this paper. On the contrary, the correction factors that would need to be applied to take into account the loss of the faintest sources in the outer and noisier region would add more systematic uncertainties at the faint end of the source counts. Furthermore, in our following analysis we consider only sources with signal to noise ratio greater than or equal to 5 (the VLA-COSMOS Large Project Catalog has been selected with a signal to noise ratio threshold of 4.5) and without a flag for possible sidelobe residuals, in order to minimize contamination from spurious sources. Given these constraints, we have a catalog of 1692 sources with  $\text{SNR} \geq 5.0$  within the inner  $1 \text{ deg}^2$  region.

The visibility area of the inner  $1 \text{ deg}^2$  of the VLA-COSMOS survey as a function of the rms noise is shown in Fig. 4. This is the area over which a source with given peak flux density (5 times the noise in our case) can be detected. Since the noise in this region is very smooth the visibility area increases very rapidly and becomes flat above an r.m.s. noise of  $\simeq 13 \mu\text{Jy}/\text{beam}$ . The same curve, computed over the entire  $2 \text{ deg}^2$ , becomes flat only above an r.m.s. noise of  $\simeq 35 \mu\text{Jy}/\text{beam}$  (see Fig. 13 in S07). This plot has been derived using the original peak flux densities and not those corrected for the bandwidth smearing since the catalog is still selected on the basis of the uncorrected peak flux.

### 3.2. The resolution bias and the intrinsic angular size distribution of sub-mJy radio sources

Besides the visibility area of each source, other correction factors need to be considered to estimate the completeness of the radio catalog and to derive the intrinsic source counts: the errors introduced by the fitting routines, the noise bias, and the resolution bias can all be modelled using simulated samples of radio sources. In particular, the resolution bias can be quite important since the beam of the VLA-COSMOS observations is  $1.5'' \times 1.4''$  (e. g. about 15 times less in area than for similar surveys carried out at the same frequency). Since the completeness of the radio catalog is defined in terms of the peak flux, while the source counts are derived as a function of the total flux density, corrections need to be applied to take into account resolved sources with peak fluxes below the catalog threshold and total flux densities above the nominal limit of the survey.

Our strategy to estimate the correction factor has been to simulate samples of radio sources, with a realistic flux density and angular size distributions, to insert these sources

in the mosaic image and to recover these mock sources using the same technique used to produce the catalog. From the comparison between the number of sources added to the image and those effectively recovered we can estimate the correction factors for different flux density bins. The correct choice of the flux density distribution is rather straightforward, as a broken power law derived from the observed distribution is a reasonable assumption, consistent with the extrapolation from shallower surveys. The choice of the angular size distribution for the simulated radio sources is more uncertain. While there is good evidence that the median of the intrinsic source size at 1 mJy is about  $2''$  and decreases with decreasing flux density at sub-mJy level, it is not known how exactly this happens and what is the best analytical relationship to model this behaviour. As we will show later, this is an important parameter in deriving the completeness of the VLA-COSMOS catalog. In the past different scaling relationships between the median angular size,  $\theta_{\text{med}}$ , and the total flux density,  $S$ , have been used, e.g.  $\theta_{\text{med}} \propto S^m$  with  $m = 0.3$  (Windhorst et al. 1990) or  $m = 0.5$  (Richards 2000).

More recently, new surveys have provided some results on the angular size distributions of the  $\mu\text{Jy}$  radio sources. Fomalont et al. (2006) obtained a complete sample of 289 radio sources with flux density  $\gtrsim 40 \mu\text{Jy}$  and found that 64% of objects are unresolved with sizes less than 1.2 arcsec. MERLIN observations at higher angular resolution ( $\sim 0.2''$ ) provided consistent results for a sample of 92 radio sources, 80 of which with flux density between  $40 \mu\text{Jy}$  and  $200 \mu\text{Jy}$  (Muxlow et al. 2005). The angular size distribution derived from the latter sample of objects, which are all resolved, shows a dominant narrow gaussian component centered at  $\simeq 0''.7$  and a tail of sources ( $\sim 20\%$  of the sample) with angular sizes between  $2''$  and  $4''$ . We derived the median of the angular size distribution for the sources observed by Muxlow et al. (2005) in the flux density range  $40\text{--}90 \mu\text{Jy}$ . The 55 sources in this flux density range have a median angular size of  $0''.7$  (with a r.m.s. dispersion of  $0''.4$ ) and a median flux density of  $54 \mu\text{Jy}$ . For comparison, Bondi et al. (2003) found that the median angular size for sources in the flux density range  $0.4\text{--}1.0 \text{ mJy}$  is  $1''.8$  with a median flux density of  $0.56 \text{ mJy}$ . The value of  $m$  consistent with these median angular sizes at different flux densities is  $m = 0.4$ . It is worth noting that this value for  $m$  has to be considered as a lower limit since the angular sizes given by Muxlow et al. (2005) are the largest angular sizes while the angular sizes given in Bondi et al. (2003) are the FWHM.

These results provide strong evidences that radio sources with flux density around  $100 \mu\text{Jy}$  have typically sub-arcsecond sizes even if the quality of the data (e.g. large number of upper limits in the angular sizes derived in Bondi et al. 2003) and the statistics (the above result on  $m$  is derived from less than 100 sources) do not allow one to derive a firm estimate of  $m$ .

Given these uncertainties, we decided to use a complementary method to derive the intrinsic angular size distribution, simulating mock samples of radio sources with different angular size distributions following a general power law  $\theta \propto S^m$  with the exponent  $m$  ranging from 0.2 to 0.5, and normalized to the integral angular size distribution derived from the VVDS survey in Bondi et al. (2003).

We constructed a simulated sample of radio sources containing about 3100 radio sources down to a total flux density level of  $30 \mu\text{Jy}$ . This allows us to count also sources with flux density below the limit which, because of positive noise fluctuations, might have a measured peak flux density above the threshold. Then, all the simulated sources were randomly injected in the inner  $1 \text{ deg}^2$  of the VLA-COSMOS mosaic and subsequently recovered using the same procedures adopted for the real sources and binned in flux density intervals. This was repeated for 3 different samples, and for four different angular size distributions (with  $m$  equal to 0.2, 0.3, 0.4, and 0.5) yielding a total of 12 simulated samples with more than 35,000 simulated radio sources. Finally, from the comparison between the number of simulated sources detected in each bin and the number of sources in the simulated input sample in the same flux density bin we derived the correction factors for each value of the exponent  $m$ . These correction factors, listed in Table 1, account for the visibility area, noise bias, fitting errors and resolution bias.

From Table 1 it is evident that for the brightest sources the correction factors are  $\lesssim 10\%$  and the differences among the correction factors for the various angular size distributions are negligible. On the other hand, below  $0.20 \text{ mJy}$  the correction factors become quite large with significant differences for the various angular size distributions. Therefore, it is important to infer the intrinsic angular size distribution in order to reconstruct the properly corrected source counts. Another interesting feature of the correction factors which is worth noting is that the maximum is not at the lowest flux density bin but around  $0.12 \text{ mJy}$ . This is due to a combination of the resolution bias and the capability to classify a radio source as resolved, which depends on the signal-to-noise ratio. A source with a given total flux density and size will be catalogued in one of the following three classes: 1) undetected, if the peak flux is below the sample threshold, 2) detected with the correct total flux density if the signal to noise ratio is high enough to allow for proper deconvolution, or, 3) detected with a lower total flux density if the signal to noise ratio is not high enough to recognize the source as resolved. The sources in the last class are assigned a total flux density lower than the intrinsic one and equal to the peak flux. A significant fraction of the sources with intrinsic total flux densities  $\lesssim 0.15 \text{ mJy}$  is redistributed to lower total flux densities since the signal-to-noise ratio is not sufficient to allow a proper deconvolution.

To constrain the intrinsic angular size distribution we performed the following test. We



derived the median major axis of the simulated samples of radio sources for each of the tested power laws ( $m = 0.2 - 0.5$ ) in the flux density range 0.25-0.4 mJy. This flux density range was chosen as a compromise to minimise the number of unresolved sources (and therefore upper limits on source size) and allow for a statistically significant large sample of sources reaching as close as possible to the lowest fluxes. We calculated both the median major axis of the original injected sources (row 1 in Tab. 2) and the median major axis of the simulated sources recovered by the fitting routine (row 2 in Tab. 2). These latter values were obtained considering also the upper limits derived for the sources fitted as unresolved ( $\lesssim 15\%$  of the total number of sources in this flux density range).

Table 2 shows that, in the flux density range 0.25-0.4 mJy, although the measured median major axis of the simulated sources is somewhat larger than that actually injected, the differences are not statistically significant for any given value of  $m$ . On the other hand, different values of  $m$  yield to significantly different median major axis.

Therefore, the value of the median major axis in this flux density range for the real sources could be used to roughly discriminate between different intrinsic angular size distributions. Unfortunately, the measured sizes of the radio sources are affected by bandwidth smearing and they can not be used for such a test. However, as we have seen in Section 2, the total flux densities are properly determined and the ratio between the total and the corrected peak flux densities can be used as an estimate of the area covered by the radio sources. Then we made the assumption that radio sources are extended in only one direction and we derived the major axis from the ratio between the total and the corrected peak flux densities. This assumption can be justified since extended radio emission is generally associated to elongated features (e.g. radio jets in AGN or spiral arms in star-forming galaxies), and when this is not true the derived source sizes will be an upper limit of the real ones. In this way we obtained a median value of the major axis for the observed sources in the flux density range 0.25-0.4 mJy of  $0''.99 \pm 0''.09$ . From the comparison with the values listed in Tab. 2, we conclude that the observed median major axis is more consistent with that obtained using simulated samples of radio sources following an angular size distribution with  $m = 0.5$  or  $m = 0.4$ .

With both methods, the comparison between the angular size distribution obtained by Muxlow et al. (2005) and Bondi et al. (2003) in different flux density intervals and the comparison between the estimate of the true angular sizes and those derived from the simulated samples, we obtained consistent results which exclude values of  $m = 0.2$  and  $m = 0.3$  and suggest  $m \simeq 0.5$ . In the following analysis we apply the correction factors obtained for  $m = 0.5$  to the radio source counts.

#### 4. The radio source counts

We have derived the radio source counts at 1.4 GHz in the inner 1 deg<sup>2</sup> region of the COSMOS field from the VLA-COSMOS catalog, corrected for the effect of bandwidth smearing and with a signal-to-noise threshold of 5. The source counts up to  $\simeq 1$  mJy are presented in Table 3. For each flux density bin we give the mean flux density, the observed number of sources, the corresponding differential source density  $dN/dS$  (in  $\text{sr}^{-1}\text{Jy}^{-1}$ ), the normalised differential counts  $(dN/dS)S^{2.5}$  (in  $\text{sr}^{-1}\text{Jy}^{1.5}$ ) with their estimated Poissonian errors, the incompleteness correction factors from Table 1 for  $m = 0.5$ , and the cumulative number of effective sources after applying the corrections. The correction factors above 0.2 mJy are  $\leq 10\%$ . Such variations are roughly consistent with the poissonian error of the source counts and for this reason the source counts above 0.2 mJy are assigned a correction factor of 1. The mean flux density in each bin was calculated as the geometric mean of the flux density extrema.

In Fig. 5 and Fig. 6 we show the raw and the corrected source counts derived from the VLA-COSMOS survey compared to those from other surveys at 1.4 GHz: the VLA-VVDS (Bondi et al. 2003), the ATCA-HDF\_S (Huynh et al. 2005), the VLA-HDF\_N (Richards 2000), the PDF survey (Hopkins et al. 2003), the SSA 13 field (Fomalont et al. 2006) and the FIRST survey (White et al. 1997). The full range of source counts up to  $\simeq 100$  mJy is shown in Fig. 5, and a blow-up of the sub-mJy region is shown in Fig.6. In both figures the raw source counts from the VLA-COSMOS survey are shown with empty circles and those corrected for incompleteness with filled ones. The solid line in Fig. 5 is a linear least-squares sixth-order polynomial fit obtained using the VLA-COSMOS source counts above 0.06 mJy supplemented with the FIRST source counts above 2.5 mJy and up to 1 Jy. The resulting polynomial fit is given by

$$\log[(dN/dS)/(S^{-2.5})] = \sum_{i=0}^6 a_i [\log(S/mJy)]^i \quad (2)$$

with  $a_0 = 0.805$ ,  $a_1 = 0.493$ ,  $a_2 = 0.564$ ,  $a_3 = -0.129$ ,  $a_4 = -0.195$ ,  $a_5 = 0.110$ , and  $a_6 = -0.017$ . The residuals from the polynomial fit have an rms of about 0.06 in the logarithm of the normalized counts. As discussed by Hopkins et al. (2003) the sixth-order polynomial is necessary to follow the different curvatures shown by the source counts. In Fig. 5 we also show for comparison with a dashed line the sixth-order polynomial fit obtained by Hopkins et al. (2003) from the Phoenix Deep Survey source counts. The two fits are in reasonably good agreement with our fit slightly higher for flux density below 0.2 mJy.

It is evident that in some cases, the field-to-field differences in the radio source counts

below 0.5 mJy are larger than the combined errors. It is likely that these differences (at least partly) can be ascribed to instrumental defects or different recipes to account for the incompleteness. In particular, the assumption of the intrinsic angular size distribution of the  $\mu\text{Jy}$  radio sources in high resolution radio surveys is certainly a factor, as we have shown in the previous Section. Nevertheless, the most extreme cases (e.g. the SSA 13 and HDF North fields) should reflect real cosmic variance (Fomalont et al. 2006).

There is a particularly good agreement between the source counts derived from the VLA-COSMOS, after correction, and the HDF-S fields. This is reassuring for the resolution bias correction we applied since the HDF-S field was observed with a resolution of about  $5''$ , and for this reason is much less affected by the precise shape of the intrinsic angular size distribution.

It is worth noting that while the VLA-COSMOS survey is not as deep as the SSA13 and HDF-N surveys, it is, by far, the one with the most robust statistics. At a flux density level of  $\sim 65 \mu\text{Jy}$  the VLA-COSMOS survey counts almost 400 sources while typical numbers for other surveys, in this flux density range, are between 50 and 90 sources.

A possible drop off in the radio source counts below  $\sim 100 \mu\text{Jy}$  has been already detected and discussed by other surveys imaging various fields with different sensitivity and resolution (Hopkins et al. 2003; Huynh et al. 2005; Fomalont et al. 2006, e.g.). Although, in every case, the drop off relies on the faintest bins it should not be immediately discounted as incompleteness in the source counts as it is accepted that the flat region of the normalised source counts below  $\sim 0.3 \text{ mJy}$  can not continue indefinitely (Windhorst et al. 1993). From the VLA-COSMOS radio source counts there is some indication that the density of sources is beginning to decrease below 100-150  $\mu\text{Jy}$  producing a downturn in the observed radio source counts, even if the result is strongly dependent on the fidelity of the first flux density bin. It is important to note that if incompleteness is responsible for the drop off observed in the first flux density bin of Fig. 6, it would mean that we are missing about 130 sources in the range 0.06-0.0735 mJy, which is extremely unlikely. So, while incompleteness at the lowest flux density levels can still be present at some level, it can not explain by itself the drop off observed in the radio source counts. Thus, this decline can provide important limits when modeling the populations contributing to the radio source counts.

As we have explained in the previous section, the intrinsic angular size distribution adopted to derive the incompleteness correction factor has a large impact in this flux density range, but adopting distributions with  $m < 0.5$  would only enhance the drop off below  $\simeq 0.15 \text{ mJy}$ .

Also the uncertainties in the bandwidth smearing correction could, in principle, sig-

nificantly modify the radio source counts and the observed drop off observed at lower flux density. We have tested this assuming two extreme cases, a constant correction over the whole area of 0.8 and 0.9 respectively. As we can expect, the first case would produce a very small difference, well within the Poissonian error boxes, since we already applied the 0.8 correction over almost 80% of the  $1 \text{ deg}^2$ . On the other hand, adopting a correction factor of 0.9 over the whole area, would significantly lower only the radio source counts in the first three bins, increasing the slope of the drop off region. As we have shown in Section 2, the assumption of a constant correction over the whole  $1 \text{ deg}^2$  is not corroborated by the real data. The data require a mixture of the two correction factors and with the previous test we have just verified that the drop off in the source counts below 0.15 mJy can not be produced by the applied smearing corrections.

We can conclude that given the large statistics and the fact that the incompleteness factors have been carefully investigated and applied, the decrease in the source counts below  $\simeq 0.10 - 0.15 \text{ mJy}$  observed in the VLA-COSMOS radio source counts should be considered real.

## 5. Summary & conclusions

In this paper we have presented a further analysis of the VLA-COSMOS Large Project Catalog with the goals of: 1) quantifying and correcting for the bandwidth smearing effect which affects the VLA-COSMOS radio mosaic and catalog; 2) determining the incompleteness of the VLA-COSMOS radio catalog, through extensive use of Monte-Carlo simulations taking into account different intrinsic angular size distributions, in order to quantify the effects of noise bias and resolution bias; 3) deriving the radio source counts at 1.4 GHz in the VLA-COSMOS field.

The bandwidth smearing correction factors have been determined from the comparison of peak and total flux densities in the final mosaic and in individual pointings where the source is within  $5'$  from the center. We have found that a two-value correction factor is a good approximation: out to a radius of  $30'$  from the center, the peak flux densities in the VLA-COSMOS catalog must be divided by a factor 0.8, while in the region between  $30'$  and  $45'$  from the center by a factor 0.9. Inside these two regions the correction factor is rather constant, within the dispersion of the data, with a sharp transition from 0.8 to 0.9 at a radial distance of  $30'$  reflecting the change in overlapping pointings. Consequently, a new classification in resolved and unresolved sources has been derived. A number of sources, originally classified as resolved, turned out to be unresolved after the bandwidth smearing correction was applied. For these sources also the total flux density was corrected.

We simulated several samples of radio sources with a flux density distribution compatible with the observed one and with different angular size distributions. The angular size distribution was modelled using  $\theta \propto S^m$  with  $m = 0.2, 0.3, 0.4, 0.5$ . These mock sources were added to the radio mosaic and recovered using the same procedure that yielded to the radio catalog. In such a way we were able to quantify the effects of the combined noise and resolution bias affecting the completeness of the radio catalog. A comparison of the median angular size at a flux density level not significantly affected by the resolution bias for the simulated samples of sources and the observed one, strongly suggest a general distribution of radio source sizes following  $\theta \propto S^{0.5}$ .

Finally, we derived the radio source counts in the VLA-COSMOS field (both uncorrected and corrected for the incompleteness). The source counts extend down to  $60 \mu\text{Jy}$  and are consistent with those derived by other surveys but with much more robust statistics. In particular, the drop off of the source counts below  $\sim 100 \mu\text{Jy}$  has to be considered real and not due to incompleteness.

The National Radio Astronomy Observatory (NRAO) is operated by Associated Universities, Inc., under cooperative agreement with the National Science Foundation. KJ acknowledges support by the German DFG under grant SCHI 536/3-1.

## REFERENCES

- Afonso, J., Georgakakis, A., Almeida, C., Hopkins, A. M., Cram, L. E. Mobasher, B., Sullivan, M. 2005, *ApJ*, 624, 135
- Benn, C.R., Rowan-Robinson, M., McMahon, R. G., Broadhurst, T.J., & Lawrence, A. 1993, *MNRAS*, 263, 98
- Bertoldi, F., et al. 2007, *ApJS*, 172, 132
- Bondi, M., et al. 2003, *A&A*, 403, 857
- Bondi, M., et al. 2007, *A&A*, 463, 519
- Capak, P., et al. 2007, *ApJS*, 172, 99
- Ciliegi, P., Zamorani, G., Hasinger, G., Lehmann, I., Szokoly, G., Wilson, G. 2003, *A&A*, 398, 901
- Ciliegi, P., et al. 2008, in preparation

- Fomalont, E.B., Kellerman, K.I., Cowie, L.L., Capak, P., Barger, A. J., Partridge, R. B., Windhorst, R. A., Richards, E. A. 2006, *ApJS*, 167, 103
- Georgakakis, A., Mobasher, B., Cram, L., Hopkins, A., Lidman, C., Rowan-Robinson, M. 1999, *MNRAS*, 306, 708
- Gruppioni, C., Mignoli, M., & Zamorani, G. 1999a, *MNRAS*, 304, 1999
- Hammer, F., Crampton, D., Lilly, S.J., Le Fevre, O., & Kenet, T. 1995, *MNRAS*, 276, 1085
- Hasinger, G., et al. 2007, *ApJS*, 172, 29
- Hopkins, A. M., Mobasher, B., Cram, L.E., & Rowan-Robinson, M. 1998, *MNRAS*, 296, 839
- Hopkins, A. M., Afonso, J., Chan, B., Cram, L. E., Georgakakis, A., Mobasher, B. 2003, *AJ*, 125, 465
- Huynh, M.T., Jackson, C.A., Norris, R.P., Prandoni, I. 2005, *AJ*, 130, 1373
- Iverson, R.J., et al. 2007, *ApJ*, 660, 771
- Lilly, S.J., et al. 2007, *ApJS*, 172, 70
- Muxlow, T.W.B., et al. 2005, *MNRAS*, 358, 1159
- Prandoni, I., Gregorini, L., Parma, P., de Ruiter, H. R., Vettolani, G., Zanichelli, A., Wieringa, M. H., Ekers, R. D. 2001 *A&A*, 369, 787
- Prandoni, I., Parma, P., Wieringa, M.H., de Ruiter, H. R., Gregorini, L., Mignano, A., Vettolani, G., Ekers, R. D. 2006 *A&A*, 457, 517
- Richards, E.A. 2000, *ApJ*, 533, 611
- Sanders, D.B., et al. 2007, *ApJS*, 172, 86
- Schinnerer, E., et al. 2004, *AJ*, 128, 1974
- Schinnerer, E., et al. 2007, *ApJS*, 172, 46 (S07)
- Scoville, N., et al. 2007, *ApJS*, 172, 1
- Scoville, N., et al. 2007, *ApJS*, 172, 38
- Seymour, N., McHardy, I.M., Gunn, K.F. 2004, *MNRAS*, 352, 131
- Simpson, et al. 2006, *MNRAS*, 372, 741

Smolčić, V., et al. 2006, MNRAS, 371, 121

Smolčić, V., et al. 2008a, ApJ in press

Smolčić, V., et al. 2008b, in preparation

Taniguchi, Y., et al. 2007, ApJS, 172, 9

Thompson, A.R., 1999 in ASP Conf. Ser. 180: Synthesis Imaging in Radio Astronomy II,  
ed. G. B. Taylor, C. L. Carilli, & R. A. Perley

Trump, J.R., et al. 2007, ApJS, 172, 383

White, R.L., Becker, R.H., Helfand, D.J., Gregg, M.D. 1997, ApJ, 475 479

Windhorst, R.A., Mathis, D., & Neuschaefer, L. 1990, ASP Conf. Ser., Evolution of the  
universe of galaxies, p.389

Windhorst, R.A., Fomalont, E.B., Partridge, R.B., Lowenthal, J.D. 1993, ApJ, 405, 498

Zamojski, M.A., et al. 2007, ApJS, 172, 468

Table 1: Correction factors for different angular size distributions

Flux bin (mJy)	$m = 0.2$	$m = 0.3$	$m = 0.4$	$m = 0.5$
0.0600-0.0735	1.29	1.19	1.06	0.99
0.0735-0.0900	1.59	1.35	1.23	1.16
0.0900-0.1103	2.12	1.81	1.53	1.36
0.1103-0.1351	2.34	2.12	1.81	1.60
0.1351-0.1655	1.60	1.46	1.32	1.29
0.1655-0.2028	1.24	1.21	1.21	1.15
0.2028-0.2484	1.05	1.03	1.00	0.99
0.2484-0.3043	1.03	1.02	0.95	0.93
0.3043-0.4564	1.10	1.08	1.09	1.07
0.4564-0.6846	1.11	1.10	1.10	1.09
0.6846-1.0270	0.98	0.98	0.97	0.98
$\geq 1.0270$	1.07	1.07	1.08	1.09

Table 2: Median major axis in the flux density range 0.25-0.4 mJy for the input and output simulated samples

Sample	$m = 0.2$	$m = 0.3$	$m = 0.4$	$m = 0.5$
	$\theta_{maj,med}$	$\theta_{maj,med}$	$\theta_{maj,med}$	$\theta_{maj,med}$
Sim. Input	$1.32 \pm 0.05$	$1.17 \pm 0.04$	$1.03 \pm 0.04$	$0.91 \pm 0.04$
Sim. Output	$1.36 \pm 0.06$	$1.24 \pm 0.06$	$1.11 \pm 0.05$	$1.00 \pm 0.05$



Table 3: The 1.4 GHz radio source counts

$S$ mJy	$\langle S \rangle$ mJy	$N$	$dN/dS$ $\text{sr}^{-1}\text{Jy}^{-1}$	$(dN/dS)S^{2.5}$ $\text{sr}^{-1}\text{Jy}^{1.5}$	$C$	$N_c(> S)$ $\text{deg}^{-2}$
0.0600-0.0735	0.066	380	$9.24 \times 10^{10}$	$3.32 \pm 0.17$	0.99	$1669 \pm 41$
0.0735-0.0900	0.081	324	$6.43 \times 10^{10}$	$3.84 \pm 0.21$	1.16	$1515 \pm 39$
0.0900-0.1103	0.100	203	$3.29 \times 10^{10}$	$3.26 \pm 0.23$	1.36	$1336 \pm 37$
0.1103-0.1351	0.122	142	$1.88 \times 10^{10}$	$3.09 \pm 0.26$	1.60	$1246 \pm 35$
0.1351-0.1655	0.150	135	$1.46 \times 10^{10}$	$3.99 \pm 0.34$	1.29	$822 \pm 29$
0.1655-0.2028	0.183	109	$9.61 \times 10^9$	$4.36 \pm 0.42$	1.15	$577 \pm 24$
0.2028-0.2484	0.224	74	$5.33 \times 10^9$	$4.02 \pm 0.47$	1.00	$393 \pm 20$
0.2484-0.3043	0.275	72	$4.23 \times 10^9$	$5.30 \pm 0.63$	1.00	$319 \pm 18$
0.3043-0.3728	0.337	45	$2.16 \times 10^9$	$4.49 \pm 0.67$	1.00	$247 \pm 16$
0.3728-0.4566	0.413	33	$1.29 \times 10^9$	$4.47 \pm 0.78$	1.00	$202 \pm 14$
0.4566-0.5593	0.505	28	$8.95 \times 10^8$	$5.14 \pm 0.97$	1.00	$169 \pm 13$
0.5593-0.6851	0.619	24	$6.26 \times 10^8$	$5.97 \pm 1.28$	1.00	$141 \pm 12$
0.6851-0.8393	0.758	12	$2.56 \times 10^8$	$4.05 \pm 1.17$	1.00	$117 \pm 11$
0.8393-1.0282	0.929	12	$2.09 \times 10^8$	$5.49 \pm 1.58$	1.00	$105 \pm 10$

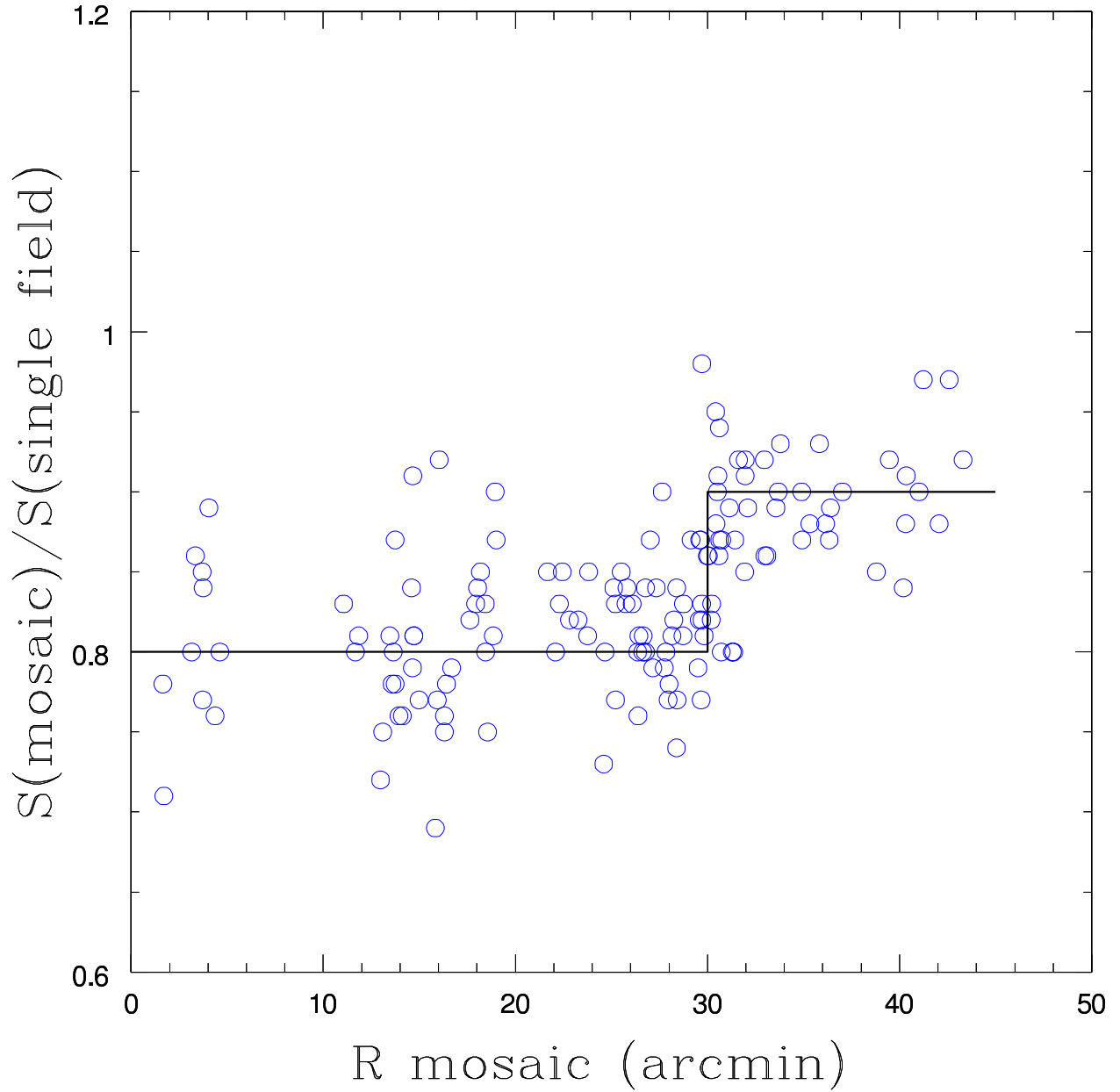


Fig. 1.— Ratio between the peak flux densities in the final mosaic and in the individual pointing where the source is within  $5'$  from the center versus the radial distance from the center in the final mosaic. Only sources with peak flux density greater than  $0.2 \text{ mJy/beam}$  and sizes smaller than  $4''$  are plotted. The straight lines at  $S(\text{mosaic})/S(\text{single pointing}) = 0.8$  and  $0.9$  for  $R < 30'$  and  $R > 30'$  show the adopted bandwidth smearing correction factors.

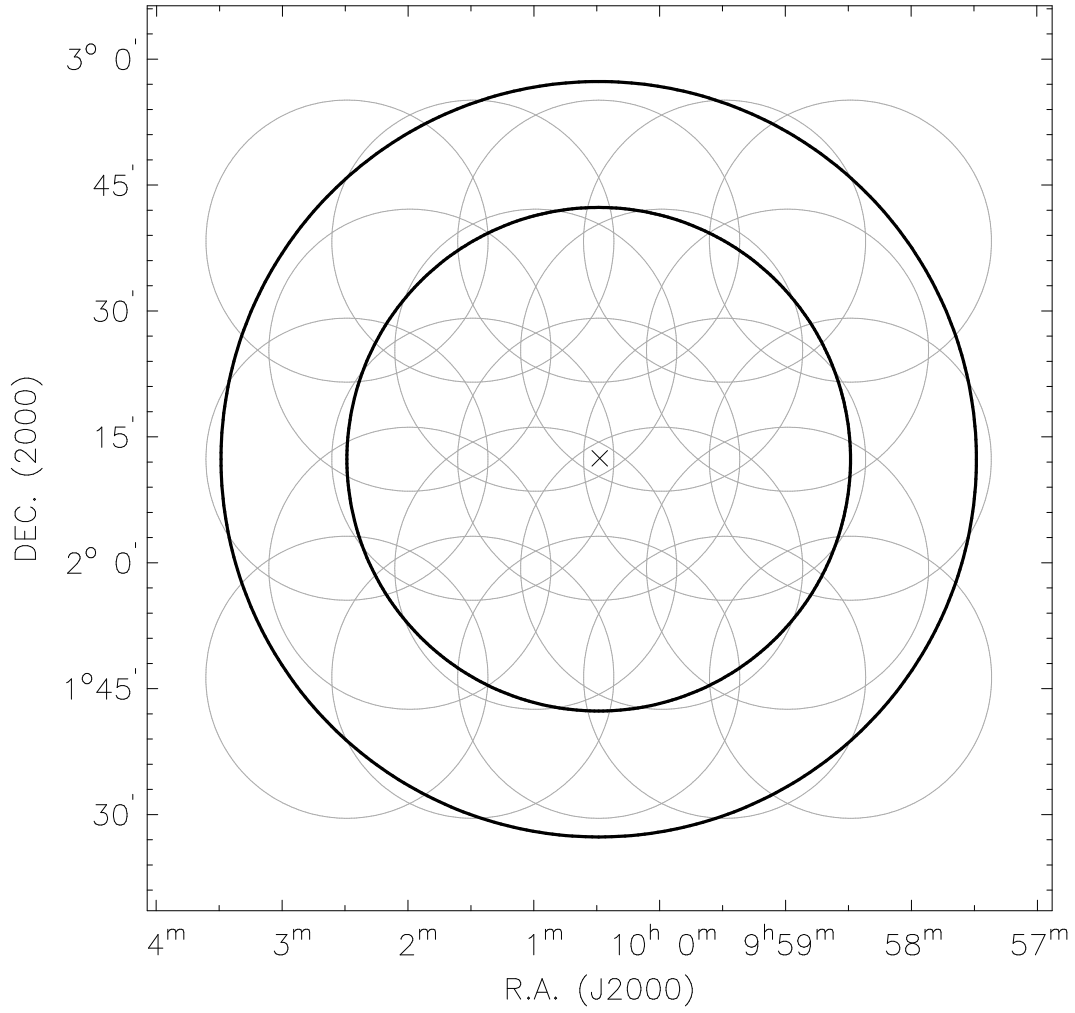


Fig. 2.— Layout of the 23 pointings for the VLA-COSMOS observations. The two circles have a radius of  $30'$  and  $45'$ .

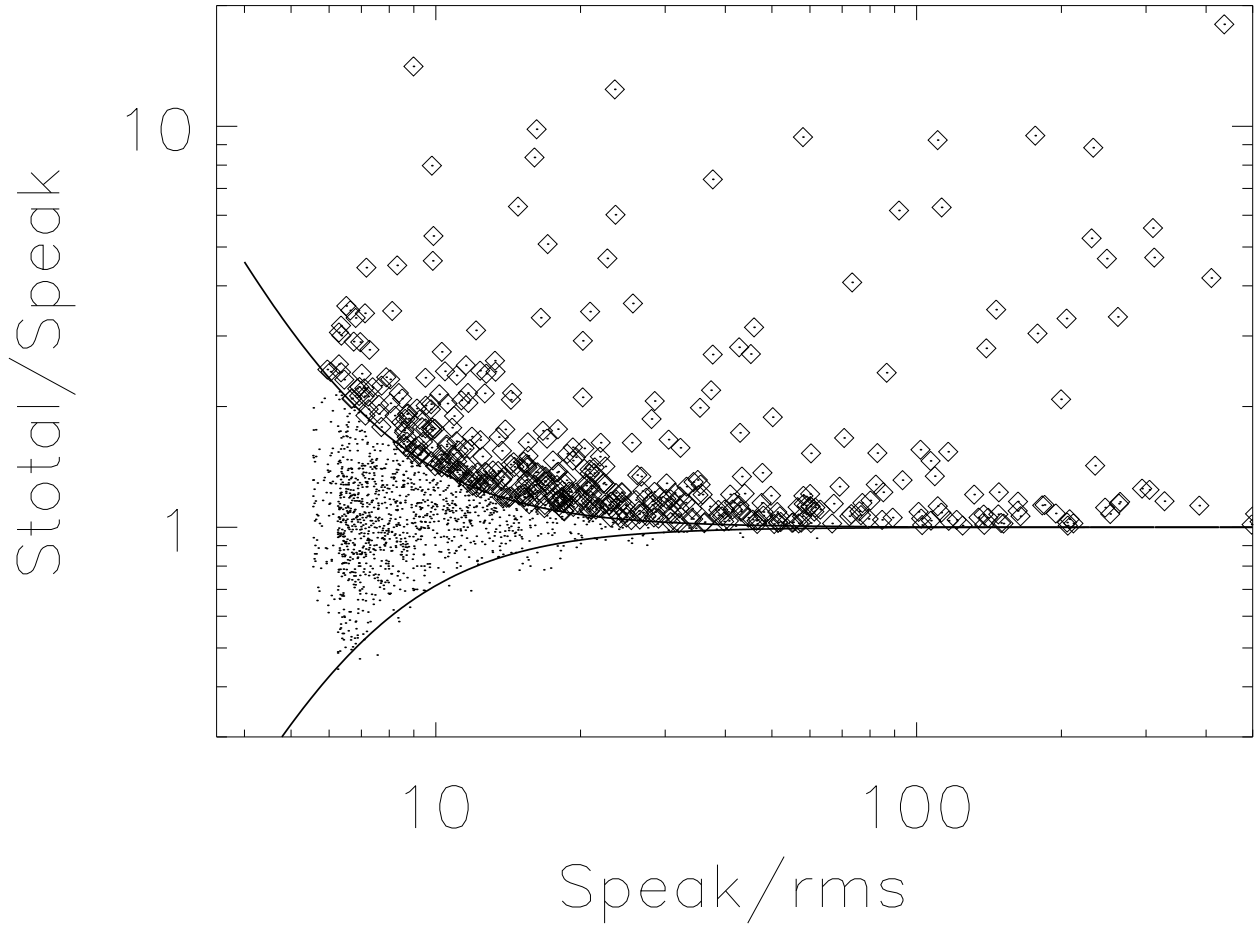


Fig. 3.— Ratio of the total flux to the corrected peak flux (see text for details) as a function of the signal-to-noise ratio. The solid lines show the upper and lower envelopes of the flux ratio distribution containing the sources considered unresolved. Open symbols show the sources considered extended. This Figure should be compared to Fig. 15 in S07.

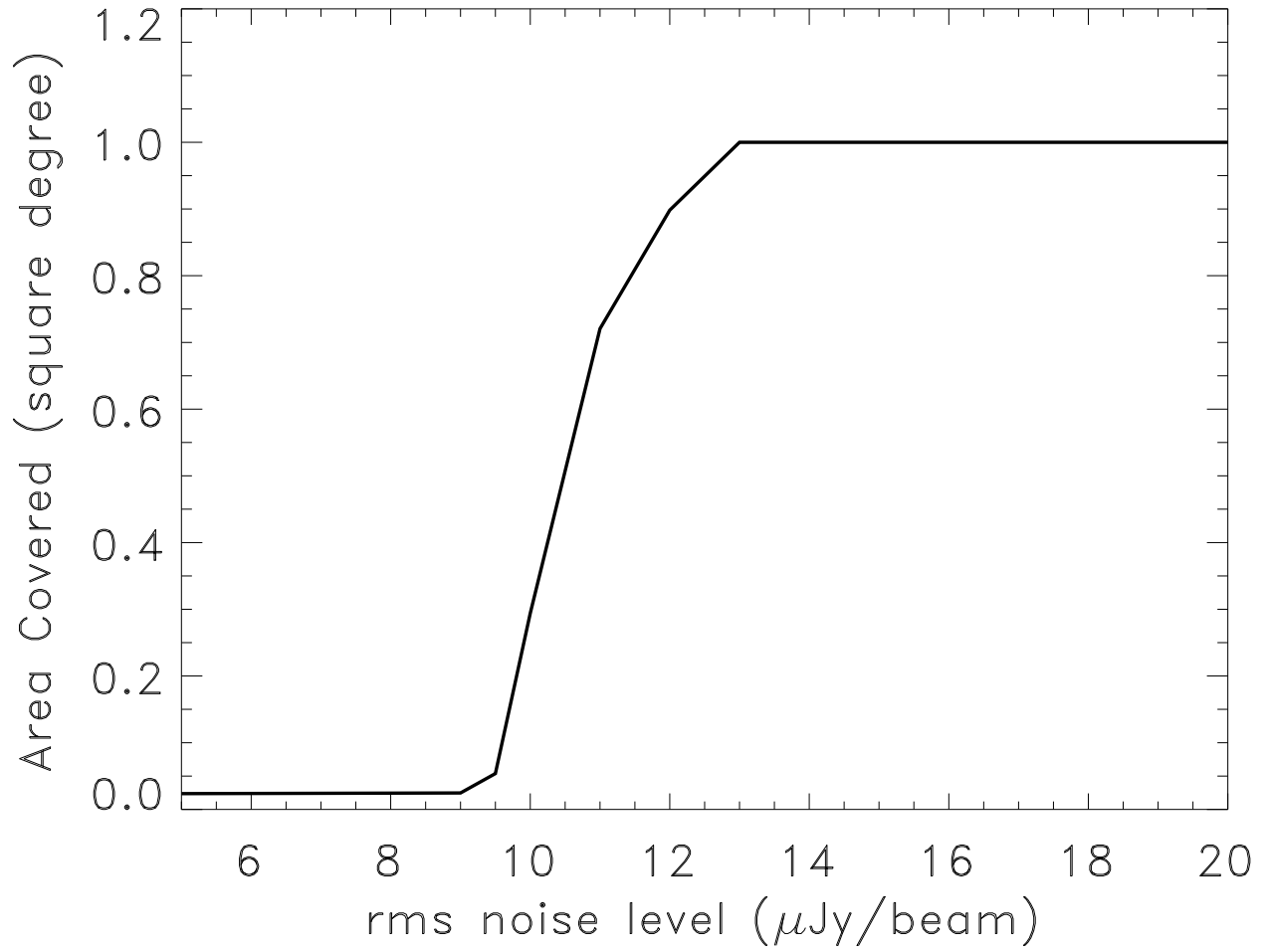


Fig. 4.— Visibility area of the inner 1 deg<sup>2</sup> of the COSMOS survey.

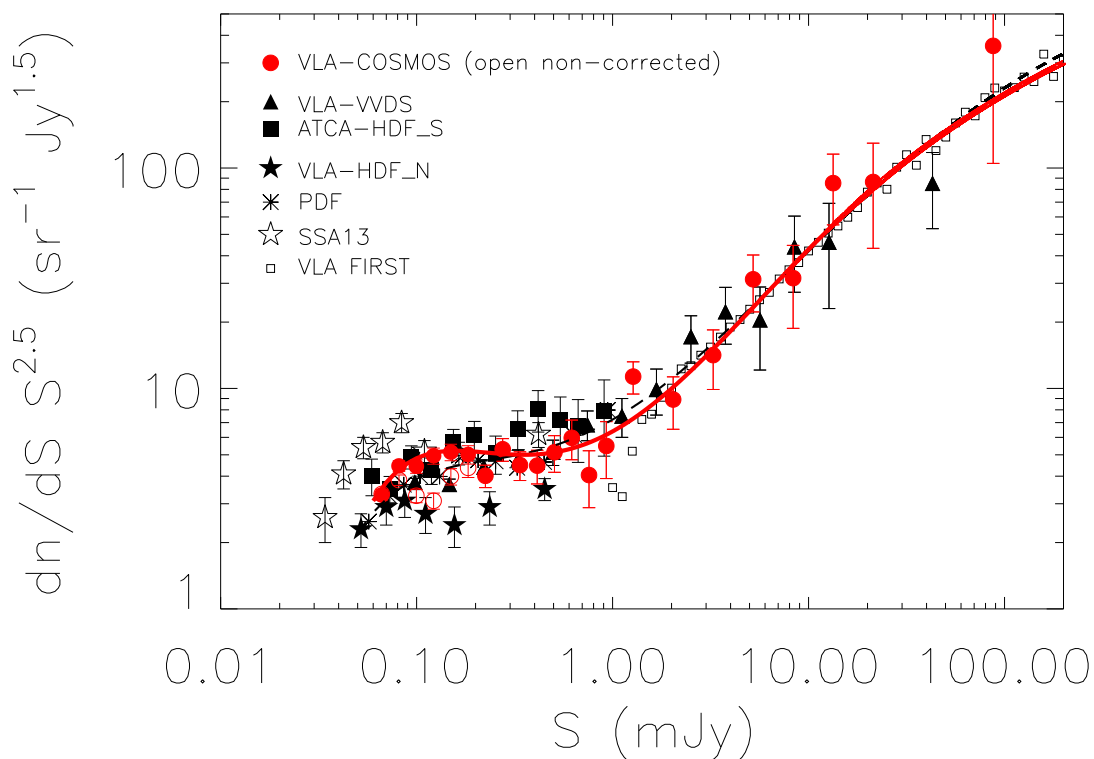


Fig. 5.— Radio source counts at 1.4 GHz from the VLA-COSMOS survey (dots) and from other surveys. Empty circles show the radio counts not corrected for incompleteness, filled circles the corrected ones using  $m = 0.5$ . The VLA-COSMOS source counts are shown along with those obtained by other deep surveys (see text). The solid line is least-squares sixth-order polynomial fit obtained using the VLA-COSMOS and the FIRST source counts. The dashed line is the fit obtained by Hopkins et al. (2003).

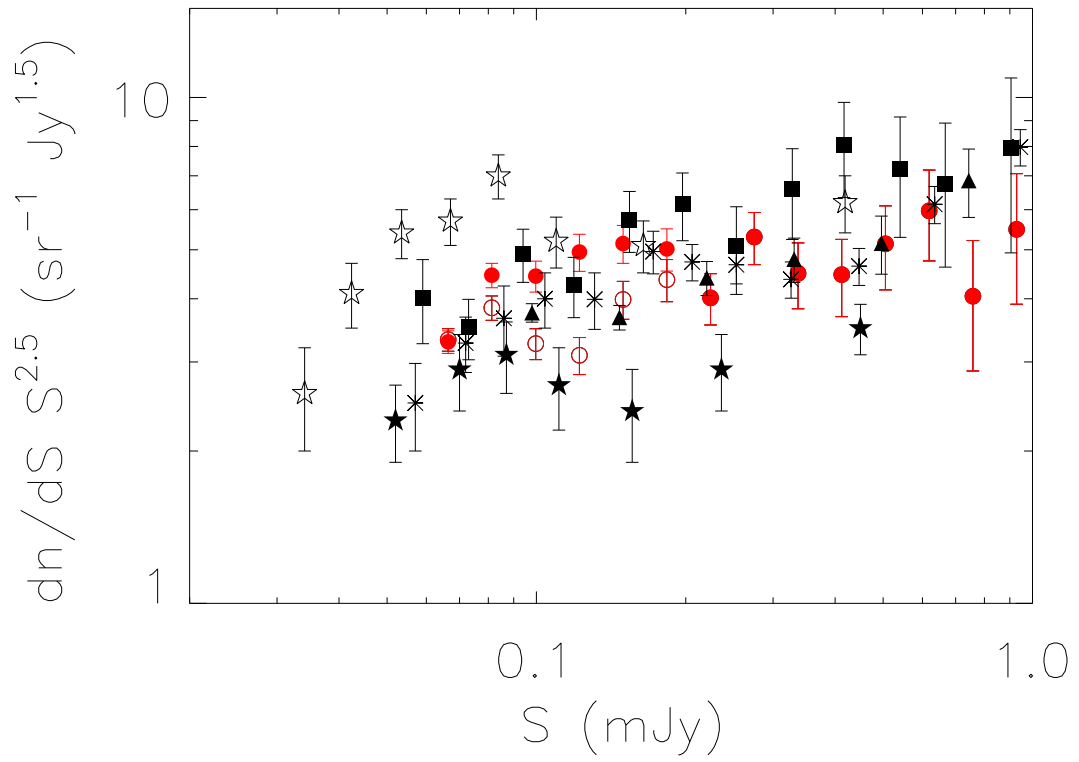


Fig. 6.— Blow-up of the radio source counts in the sub-mJy region. Symbols are the same as in Fig. 5.